Check for updates

Nano-composites and Smart Materials: Design, Processing, Manufacturing and Applications-Original Research Article

ADVANCED COMPOSITES LETTERS

Advanced Composites Letters
Volume 29: 1–14
© The Author(s) 2020
DOI: 10.1177/2633366X20963137
journals.sagepub.com/home/acm
SAGE

Investigating the influence of WEDM process parameters in machining of hybrid aluminum composites

Amresh Kumar[1], Neelkant Grover[2], Alakesh Manna[3], Jasgurpreet Singh Chohan[4], Raman Kumar[4], Sunpreet Singh[5], Chander Prakash[6] and Catalin Iulian Pruncu[7,8]

Abstract

This article presents an experimental investigation to assess the influence of input process parameters of machinability of wire electrical discharge machining (WEDM) process for machining of triple-reinforced silicon carbide, graphite, and iron oxide hybrid aluminum (Al-6061) metal matrix composites. The composite work specimens, developed using stir casting process, have been processed through WEDM process by adopting a statistically controlled design of experimentation approach. Furthermore, analysis of variance and regression analysis have been performed to understand the influence of the input process parameters on material removal rate (MRR) and spark gap (SG) width. The statistical analysis highlighted the improvements in MRR and SG by 33.72% and −27.28%, respectively, upon adopting the suggested optimized range of input process parameters. Further, the morphology of the machined composite surfaces has also been studied using scanning electron microscopy and energy dispersive spectroscopy to report the phenomenon of formation of recast layer.

Keywords

aluminum composites, optimization, wire EDM, recast layer, ANOVA, regression analysis

Introduction

The ever growing demand of materials designed to exhibit exceptional properties imperatively needed for numerous industrial applications has posed strenuous challenge to the researchers. Having witnessed a limited potential being exhibited by conventional materials, the metal matrix composites (MMCs) have become subject of key interest for practicing engineers owing to their tailor-made material properties combinations especially desired to cope up the necessitates of aviation, automotive, and defense industries.[1,2] Notably, particulate-reinforced MMCs offer high strength/weight ratio, high stiffness, and good wear resistance over monolithic materials, therefore offer potential commercial prospectus.[3,4] Recently, the hybrid MMC materials proved to be more attractive properties and these materials are fabricated by embedding matrix phase with two or more reinforcements to improve engineering properties.[5] The unique properties of hybrid aluminum (Al) matrix composites are intended for a wide range of applications, such as aircraft and fighter plane components,

[1] Department of Mechanical Engineering, Chandigarh Engineering College, Landran, Punjab, India
[2] Department of Mechanical Engineering, IKG-PTU Campus, Kapurthala, Punjab, India
[3] Department of Mechanical Engineering, Punjab Engineering College, Chandigarh, India
[4] Department of Mechanical Engineering, Chandigarh University, Mohali, Punjab, India
[5] Department of Mechanical Engineering, National University of Singapore, Singapore
[6] School of Mechanical Engineering, Lovely Professional University, Punjab, India
[7] Department of Mechanical Engineering, Imperial College of London, London, UK
[8] Design, Manufacturing & Engineering Management, University of Strathclyde, Glasgow, Scotland, UK.

Date received: 17 June 2020; accepted: 9 September 2020

Corresponding author:
Catalin Iulian Pruncu, Department of Mechanical Engineering, Imperial College of London, London, UK.
Email: c.pruncu@imperial.ac.uk

Creative Commons CC BY: This article is distributed under the terms of the Creative Commons Attribution 4.0 License (https://creativecommons.org/licenses/by/4.0/) which permits any use, reproduction and distribution of the work without further permission provided the original work is attributed as specified on the SAGE and Open Access pages (https://us.sagepub.com/en-us/nam/open-access-at-sage).

drive shafts, brake rotor, airframe structure, and automobile components (such as piston, cylinder liner, engine block, turbocharger, supercharger, valve gears, brackets, etc.). These materials can be fabricated by different methods, including liquid-metallurgy methods, solid-state consolidation technique, and deposition of matrix from a vapor or semisolid phase.[3] In particular, the liquid-metallurgy approach is highly attractive for fabricating composites, wherein the liquid stir casting process has been recognized as one of the most viable and economic methods to fabricate particulate-reinforced composites.[4,6,7] Reportedly, the manufacturing industries are keen in investing for improving the methods to produce economical and precise mechanical components which otherwise may not be possible without considering the importance of machining processes. Manufacturing industries primarily rely on turning, drilling, and milling and other conventional machining methods for processing of the materials. Owing to the presence of reinforcements such as aluminum oxide (Al_2O_3), silicon carbide (SiC), and boron carbide, which are hard and sometimes even harder than tool material and highly abrasive, the processing of MMCs proves to be an uphill task since their existence. The major challenge arises in machining of MMCs, when de-bonded particles come between tool edge and work surface; it subsequently causes rapid tool wear, poor surface integrity, and burr formation.[8–10] The ploughed particles through the matrix form grooves and scratches.[11] Further, matrix tearing may take place during surface generation when the cutting tool faces agglomerated reinforcements. Increase in size of ceramic particle also enhances tool wear[12,13] which further reduces the surface finish of machined surface. This observation was further substantiated by Kannan and Kishawy[13] while machining the composites with 10 vol% alumina particles in an Al-6061 matrix wherein increased size was accounted for significant damage to tool and machined surfaces. Many authors recommended the use of polycrystalline diamond (PCD) tools to reduce the deterioration of the machined surface as these tools are less prone to wear among available tool materials, but high cost associated with them limits their use.[14–16] PCD tools exhibits chipping damage due to its sharp cutting edge by impact of loosened ceramic particles from the spinning MMC work piece.[13,16] Alternatively, MMCs can be machined using nontraditional machining approaches, such as laser cutting, water jet machining, and electrical discharge machining, without considering the physical properties of MMCs. The wire electrical discharge machining (WEDM) has been proved as an efficient machining process to machine these materials achieving reasonably good precision and economy.[17,18]

Yue and Dai[19] adopted a strategy by varying one factor at time to explore machining behavior of Al/Al_2O_3 MMCs. They found that the sizes of particles had significant influence in determining the banding and surface roughness (SR). The fiber-reinforced composites were found to be machined to a better surface finish than particle-reinforced MMC. The authors also reported that machined surface of MMC was inferior to the unreinforced Al matrix under fine cutting conditions. Gatto and Iuliano[20] carried out an experimental investigation to determine WEDM machinability of Al/SiC composites and didn't observe the presence of SiC particulates in the recast layer of machined work material. Rozenek et al.[21] studied the WEDM of MMCs and highlighted that the cutting speed for machining a reinforced metallic composite should be considerably lower than the pure matrix. Yan et al.[22] performed experiments to machine alumina-reinforced Al matrix using a computerized WEDM process. It has been found that the high wire speed, low wire tension, and high flushing rate are some of the vital process parameters to prevent the wire breakage. Manna and Bhattacharyya optimized the WEDM parameters in response to material removal rate (MRR) and SR and proposed mathematical relations to establish improved machinability criterion.[9] Further, Patil and Brahmankar[23] investigated that during WEDM of Al matrix composites, the disintegration of alumina particles from the machined surface has deteriorated the desired surface finish of machined workpiece. It has been reported that an increase in the percentage of the reinforcement can render narrower kerf profile on machined samples.[24] Apart from this, other defects such as wire breakage, black spots, and cracks can also prominently deteriorate the machined surface textures during WEDM processing.[25] The vigilant examination of spark eroded surface shown that the poorest surface structure occupied with large number of cavities and enlarged craters is predominantly due to the higher pulse-on-time and lesser volume of nano-SiC in composites.[26] The close examination of cross section of the wire electrode clearly indicated the influence of reinforcement size on degradation of brass wire electrode. A severe degradation has been noticed at the curved edge at the front and straight edge side which participates in cutting of MMCs.[27]

Besides other control parameters of interest, the type of ceramic reinforcements is also an important attribute influencing performance measure. Satishkumar et al.[28] performed the L_9 (orthogonal array (OA))-based machining experiments on three variants of MMC material reinforced with particulates of SiC in vol. fraction of 5%, 10%, and 15%, respectively, and examined the WEDM characteristics of the process. The analysis of variance (ANOVA) method was employed to draw a conclusion from the results of experiments. The researchers verified through experiments that SiC% was crucial factor to determine the SR of machined samples. It has been reported further that ceramic particles shield the matrix materials from intense heat of discharge thus influencing erosion rate, surface characteristics, and taper of kerf.[29] It has been found that the recent studies are oriented toward the investigation of the machinability prospects of differently reinforced hybrid MMCs.[30–33] Despite the availability of the broad range of

Table 1. Properties of Al-matrix (AA 6061) and hybrid Al-MMC.

Materials	Density (g/mm^3)	Hardness (BHN)	Ultimate tensile strength (MPa)
Pure AA6061 alloy	2.71	88	267
Hybrid Al composite	2.76	96.8	290.1

Al: aluminum; MMC: metal matrix composite; BHN: Brinell hardness number.

research activities in the themed research, the two existing research gaps are as follows:

- There are very limited studies available on the optimization of the differently hybrid metal composites.
- The phenomenon of the formation of recast layer during WEDM of hybrid MMCs is not addressed.

On the basis of the literature review, the authors have been persuaded to conduct the experimental investigation to suggest the optimal machining parameters for effective machining of stir casted hybrid Al-MMC subjected to attain maximum MRR and minimum spark gap (SG) for considered range of control parameters. The current research article broadly presents a comprehensive procedure to figure out optimal settings of machining parameters based upon the design of experimentation approach. Besides indicating the outcome of signal/noise (S/N) ratio analysis and ANOVA, the research article indeed purposes the mathematical models which are developed to correlate the machining response characteristics with machining control parameters. The machined surface textures have been analyzed through scanning electron microscopy (SEM) and energy dispersive spectroscopy (EDS) analysis to further explain the phenomenon of formation of recast layer during machining.

Fabrication of hybrid Al-MMC

The fabrication of differently reinforced hybrid aluminum (AA6061) matrix composites has been prepared through liquid stir casting process. The particulate reinforcements, such as SiC, graphite (Gr), and iron oxide (Fe_2O_3), have been selected in percentage weight proportions of 10%, 3%, and 3%, respectively. Three furnaces of capacity 1250°C, 1050°C, and 550°C were simultaneously used for melting of Al-6061 alloy, preheating of SiC, Gr, and Fe_2O_3 reinforcements, and baking of clay coated metal mold cavity, respectively, during casting of hybrid composites. The resistance heating furnace equipped with temperature regulator/indicator was used for stir casting of hybrid MMC samples. The melting was performed in a Gr crucible. A Gr stirrer and a three-blade impeller were mounted at 120° × 45° to stir the melt mixture and uniformly mix the reinforcements. An electric motor was used to control the stirring speed and to create a vortex flow. For sound castings, effective stirring of the molten mixture is highly important to achieve uniform mixing of constituents. The stir casted samples were tested for their mechanical properties, such as hardness and tensile strength, refer Table 1. Further, Figure 1(a) to (c) shows the SEM and EDS results of differently reinforced hybrid composite (polished sample). The SEM image has been captured at an accelerating voltage and magnification of 20 kV and 1000×, respectively. It can be seen in Figure 1 that the overall surface area on selected region has identified the presence of Al as major element along with Si, Gr (allotrope of C), and Fe (allotrope of Fe_2O_3). The mechanical properties of the cast samples were tested as per standard procedure explained elsewhere.[34]

WEDM of hybrid Al-MMC

Planning for experimentation

Electronica Sprintcut-734 WEDM (Electronica India Limited) was used for machining of work material. Performance measures, namely, MRR and SR heights, were recorded while performing WEDM machining experiments. The work material, tool electrode, and the other machining conditions were considered for experiments as follows:

- Work-piece: Hybrid Al-MMC (anode).
- Thickness: 12 mm.
- Programmed size of the workpiece: 5 × 5 × 12 mm^3.
- Tool: Brass wire electrode of 250 μm (cathode).
- Dielectric fluid: deionized water (temperature: 22–25°C).
- Flushing pressure of deionized water: 14.5 kg/cm^2.
- Specific resistance of deionized water: 1–3 mA.
- Peak voltage (VP): 100 V.

A set of preliminary experiments were carried out to set the level of the various parameters of WEDM. Based on the acquired results from preliminary experiments six parameters, such as: pulse peak current (I_p), pulse-on-time (T_{on}), pulse-off-time (T_{off}), wire feed rate (W_F), wire tension (W_T), and SG-set voltage (SV) are selected. The levels of the identified input process parameters are given in Table 2.

To produce the desired profile on the workpiece, a minimum SG is desired to ensure precise cut in WEDM process especially components demanding close tolerances. It is evident that when the wire electrode travels without any offset along the programmed path, the actual size of the machined workpiece becomes undersize. Therefore, it is essential to compute the wire offset to make the correction in the path profile of wire in the CNC program.[35] So,

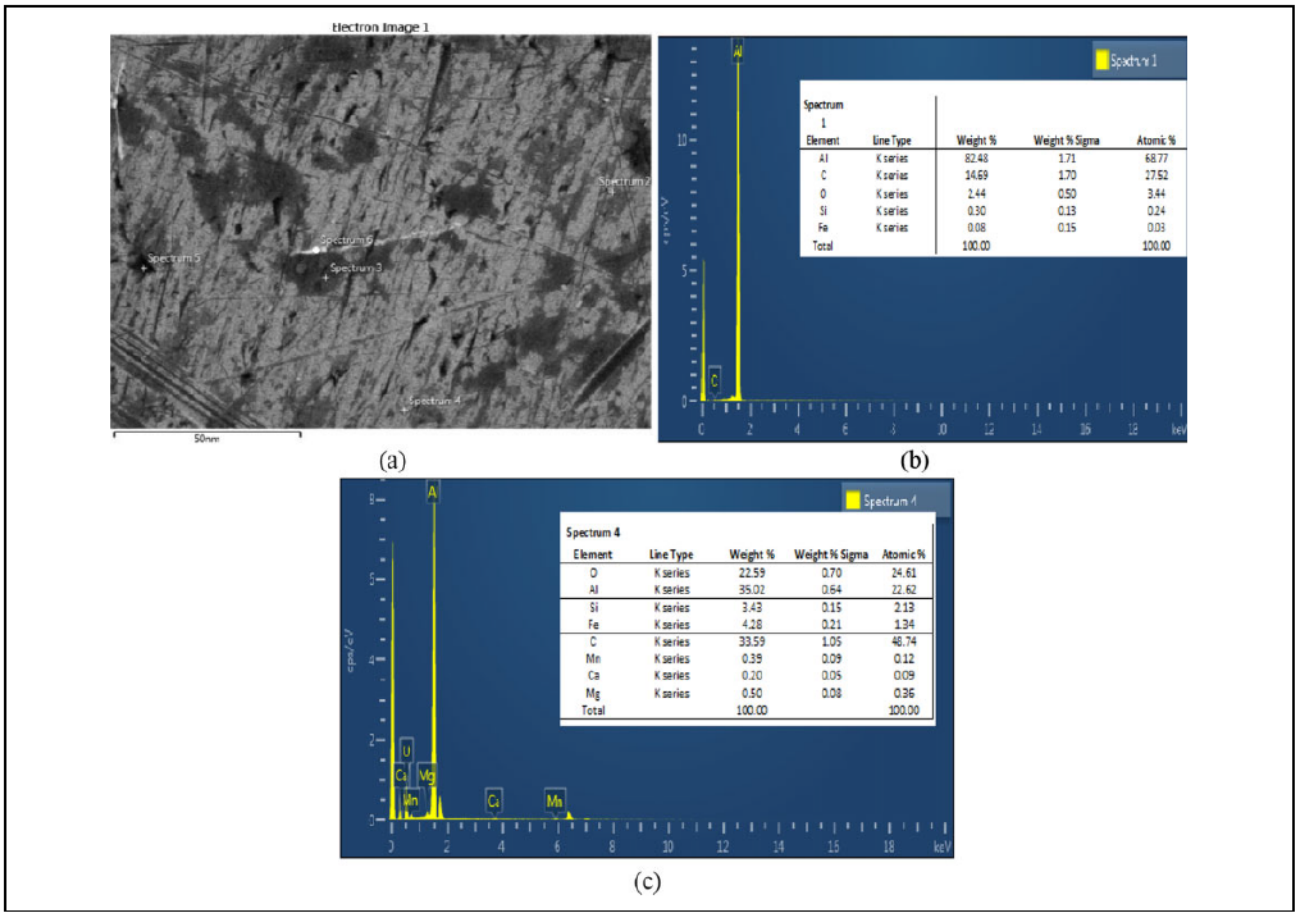

Figure 1. Scanning electron microscopic image and EDS analysis of stir casted hybrid Al-MMC. EDS: energy dispersive spectroscopy; Al: aluminum; MMC: metal matrix composite.

equation (1) has been used to determine the SG width (W_g; µm), as follows

$$2W_g + d = b \tag{1}$$

where b is the width of cut in millimeters and d is the diameter of the brass electrode (250 µm). The width of slot formed between outer surface of cut work piece and inner surface of remainder composite after machining experiment was measured at five locations using TESAMASTER micrometer (EuroPac Precision).

The MRR (mm^3/min) for each set of experiment has been calculated using equation (2)[17]

$$\mathrm{MRR} = C_m \times b \times h \ [\mathrm{mm}^3/\mathrm{min}] \tag{2}$$

The mean cutting speed (C_m; mm/min) was recorded from the display screen of the Sprintcut WEDM machine during experiment. The height of workpiece "h" and width of cut "b" were also measured using micrometer.

Design of experiments

The scrutiny of appropriate OA used in this experimentation was determined through calculation of the total degrees of freedom (DoFs). The DoF is based on the levels of each individual control parameters and considered interaction between design parameters. Based on the calculated DoF, the $L_{27}(313)$ OA was selected which enabled to conduct the 27 machining experiments. The optimal level of a process parameter is the level which results in the highest value

Table 2. WEDM parameters and their levels considered for experiments.

S. No.	Input parameters	Level 1	Level 2	Level 3	Unit
1	A *Pulse peak current* (I_p)	80	100	120	A
2	B *Pulse-on-time* (T_{on})	0.5	0.8	1.1	µs
3	C *Pulse-off-time* (T_{off})	20	16	12	µs
4	D *Wire feed rate* (W_F)	5	7	9	m/min
5	E *Wire tension* (W_T)	850	1000	1200	G
6	F *Spark gap-set voltage* (SV)	25	30	35	V

WEDM: wire electrical discharge machining; I_p: pulse peak current; T_{on}: pulse-on-time; T_{off}: pulse-off-time; W_F: wire feed rate; W_T: wire tension; SV: set voltage.

Table 3. Control log of experimentation.

	Control parameters						Response parameters			
							Average values		S/N ratios (dB)	
Exp. No.	I_p	T_{on}	T_{off}	W_F	W_T	SV	MRR (mm^3/min)	SG (mm)	MRR	SG
1	80	0.5	20	5	850	25	5.212	0.016	14.320	35.809
2	80	0.5	20	5	1000	30	5.126	0.017	14.151	35.650
3	80	0.5	20	5	1200	35	5.561	0.017	14.901	35.340
4	80	0.8	16	7	850	25	6.560	0.019	16.338	34.563
5	80	0.8	16	7	1000	30	8.672	0.021	18.760	33.473
6	80	0.8	16	7	1200	35	8.122	0.022	18.191	33.239
7	80	1.1	12	9	850	25	9.351	0.023	19.416	32.728
8	80	1.1	12	9	1000	30	9.651	0.023	19.690	32.617
9	80	1.1	12	9	1200	35	9.190	0.024	19.266	32.465
10	100	0.5	16	9	850	30	7.560	0.021	17.570	33.637
11	100	0.5	16	9	1000	35	7.678	0.021	17.705	33.769
12	100	0.5	16	9	1200	25	7.561	0.022	17.571	33.112
13	100	0.8	12	5	850	30	11.451	0.023	21.176	32.692
14	100	0.8	12	5	1000	35	12.212	0.024	21.734	32.287
15	100	0.8	12	5	1200	25	11.134	0.023	20.929	32.727
16	100	1.1	20	7	850	30	9.567	0.025	19.615	32.006
17	100	1.1	20	7	1000	35	9.107	0.024	19.180	32.287
18	100	1.1	20	7	1200	25	8.972	0.023	19.0578	32.727
19	120	0.5	12	7	850	35	8.601	0.022	18.690	33.112
20	120	0.5	12	7	1000	25	7.712	0.024	17.729	32.578
21	120	0.5	12	7	1200	30	7.515	0.024	17.501	32.432
22	120	0.8	20	9	850	35	8.567	0.024	18.656	32.359
23	120	0.8	20	9	1000	25	8.401	0.025	18.485	32.111
24	120	0.8	20	9	1200	30	8.756	0.024	18.846	32.468
25	120	1.1	16	5	850	35	9.678	0.025	19.715	32.006
26	120	1.1	16	5	1000	25	10.167	0.025	20.143	32.111
27	120	1.1	16	5	1200	30	9.567	0.025	19.615	31.937

I_p: pulse peak current; T_{on}: pulse-on-time; T_{off}: pulse-off-time; W_F: wire feed rate; W_T: wire tension; SV: set voltage; MRR: material removal rate; SG: spark gap.

of S/N ratio transformation. In the Taguchi method S/N ratio (dB), the term "signal" stands for the undesirable value (SD) for the output characteristic. The S/N ratio defined in mathematical aspect as the higher-the-better (i.e. maximize, example: MRR) is described

$$\eta = -10\log_{10}\frac{1}{n}\sum_{i=1}^{n}\frac{1}{y_i^2} \tag{3}$$

while for lower-the-better (i.e. minimize, example: SG)

$$\eta = -10\log_{10}\frac{1}{n}\sum_{i=1}^{n}y_i^2 \tag{4}$$

where S/N ratio (dB) denoted by η computed from experimentally observed values; y_i is termed as the experimentally acquired response of the ith machining experiment, while n is the number of repetitions of each machining experiment.[12] Utilized the acquired results, calculated the S/N ratio and drawn S/N ratio graphs for optimization of WEDM parameters for different response characteristics.

Results and discussion

Table 3 represents the raw data and S/N ratio obtained for MRR and SG. As per the Taguchi method, the significant parameters can be identified through ANOVA. The results developed through mathematical models bear the relationship between WEDM control and response parameters. Figure 2 shows the S/N ratio (dB) graphs for MRR indicating the influence of the different levels of the control parameters. Notably, the optimal level of machining control parameter is identified to be peak S/N ratio plot. Based on Figure 2, the optimal condition that can yield maximized MRR is identified to be $A_2B_3C_1D_3E_2F_3$ (i.e. parameter A_2 (level 2, S/N = 19.39), parameter B_3 (level 3, S/N = 19.52), parameter C_1 (level 1, S/N = 19.57), parameter D_3 (level 3, S/N = 18.58), parameter E_2 (level 2, S/N = 18.62), and parameter F_3 (level 3, S/N = 18.67)). Further, Table 4 represents the ANOVA and F-test values with contribution of each WEDM parameters for MRR. The significance of each machining parameter can be determined using ANOVA.[36,37] Table 4 also represents the most significant (marked by the superscript letter b) and significant (marked by the superscript letter a) WEDM

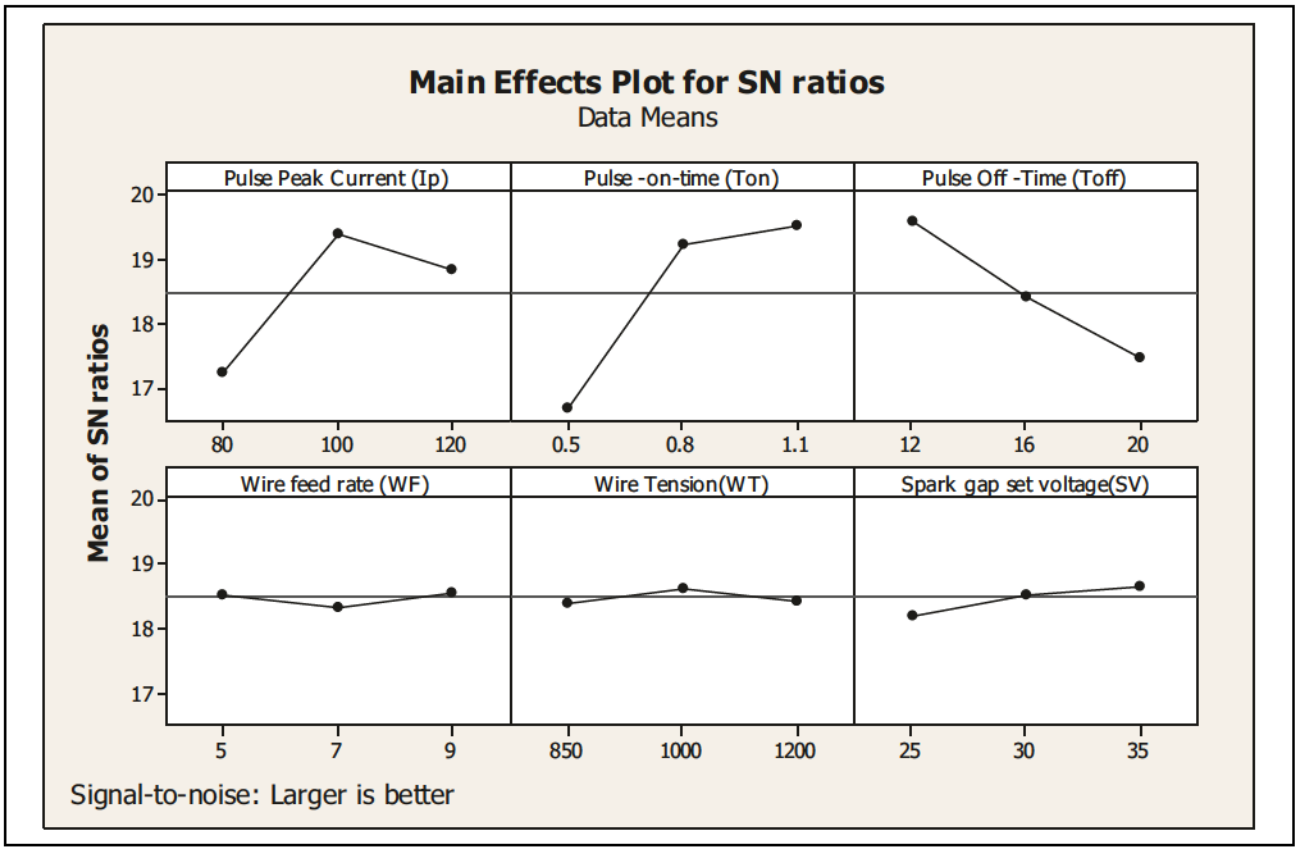

Figure 2. S/N ratio plot for MRR. S/N: signal/noise; MRR: material removal rate.

Table 4. ANOVA for MRR.

Source	Degree of freedom	Sum of square	Variance	*F*-test	Probability	Contribution (%)
I_P	2	18.166	9.0833	39.56	0.000	23.30
T_{on}	2	36.261	18.1305	78.96	0.000	46.50
T_{off}	2	17.567	8.7839	38.26	0.000	22.53
W_F	2	1.5824	0.7912	3.45	0.061	2.03
W_T	2	0.3704	0.1852	0.81	0.466	0.48
SV	2	0.8121	0.4060	1.77	0.207	1.04
Residual error	14	3.2145	0.2296			4.12
Total	26	77.973				100.00

ANOVA: analysis of variance; MRR: material removal rate; I_p: pulse peak current; T_{on}: pulse-on-time; T_{off}: pulse-off-time; W_F: wire feed rate; W_T: wire tension; SV: set voltage.

parameters for MRR concerning the machining of hybrid Al-MMC.

From Table 4, it can clearly be figured out that pulse-on-time had most significant effect on MRR with contribution of 46.50%. Further, the pulse-peak current and the pulse-off-time have been noticed to be statistically significant with contribution of 23.30% and 22.53%, respectively. Along with these, the wire feed rate can also be not ignored as it has *F*-test value of 3.45, with a contribution of about 2.03% in MRR.

The setting of current and pulse duration affects the spark intensity and hence the MRR.[38] Figure 2 illustrates that the MRR escalates as pulse peak current amplifies from 80 A to 100 A. However, a drop in MRR has been witnessed when pulse peak current amplifies from 100 A to 120 A. This discrete trend emerged owing to stochastic nature of the WEDM process. The material removal mechanisms, such as sparking, melting, vaporizing and removal of material by impulsive force, have been activated during rapid and repetitive sparking in WEDM. It became more effective when machining was carried out at moderate level of peak current. Further, at high level of peak current, MRR was dropped slightly on account of contamination of gap caused by increased number of debris and dislodged ceramic reinforcements. Machining

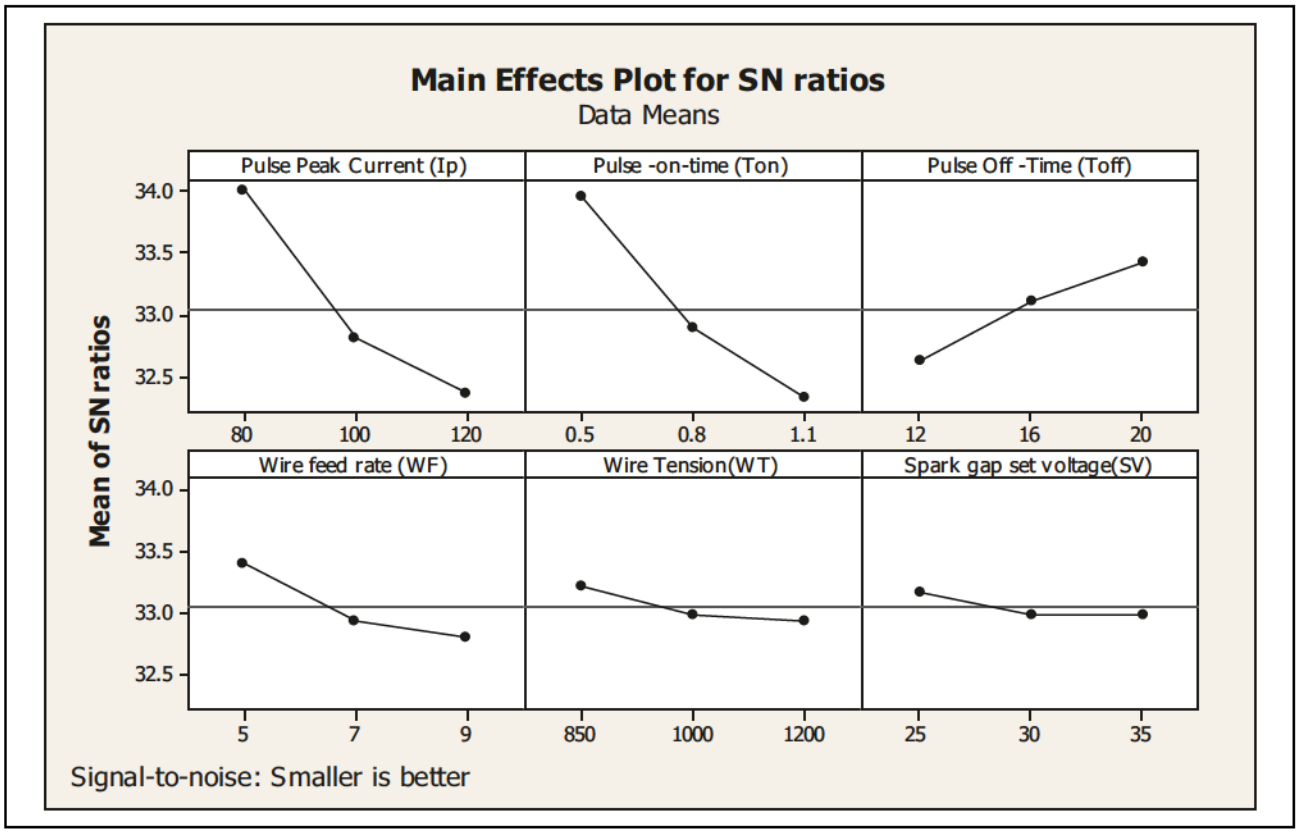

Figure 3. S/N ratios plot for SG. S/N: signal/noise; SG: spark gap.

Table 5. ANOVA for SG.

Source	Degree of freedom	Sum of square	Variance	*F*-test	Probability	Contribution (%)
I_p	2	0.0000739	0.000037	53.02	0	41.45
T_{on}	2	0.0000708	0.0000354	50.79	0	39.71
T_{off}	2	0.0000136	0.0000068	9.75	0.002	7.63
W_F	2	0.000007	0.0000035	5.03	0.023	3.93
W_T	2	0.0000021	0.000001	1.48	0.26	1.18
SV	2	0.000001	0.0000005	0.75	0.492	0.56
Residual error	14	0.0000098	0.0000007			5.50
Total	26	0.0001783				100.00

ANOVA: analysis of variance; SG: spark gap; I_p: pulse peak current; T_{on}: pulse-on-time; T_{off}: pulse-off-time; W_F: wire feed rate; W_T: wire tension; SV: set voltage.

experiments at longer spark duration, such as more expansion in plasma channel, enhance melting of material per spark in the gap. Hence, amplification of pulse-on-time results in augmented MRR. Figure 2 also depicts the influence of pulse-off-time upon MRR. Since no sparking takes place during pulse-off-time interval, the MRR was expected to drop. A sharp reduction in MRR was noticed at peak pulse-off-time owing to reduced frequency of sparks for a specific period of machining cycle. The S/N ratio plot for MRR further demonstrates that the MRR is highest at the moderate setting of wire tension. Machining at different levels of wire feed rate as well as SG-SV caused a marginal deviation in MRR.

In case of SG, refer Figure 3 for S/N ratio plot, the parametric combination for obtaining minimum SG has been observed as $A_1B_1C_3D_1E_1F_1$. It means that the best parametric level for parameter A: level 1 and S/N 33.99 dB, B: level 1 and S/N 33.94 dB, C: level 3 and S/N 33.42 dB, D: level 1 and S/N 33.4 dB, E: level 1 and S/N 33.21 dB, and F: level 1 and S/N 33.16 dB. The ANOVA results for the SG are displayed in Table 5 and depict the influence of the input control parameters. It has been found that the most significant factors for SG are pulse peak current (53.02%) and pulse-on-time (50.79%). Likewise, pulse-off-time and wire feed rate also influence the SG, significantly.

S/N ratio graph illustrates that SG exhibited a linear trend with pulse peak current and pulse-on-time. It further indicates that high level setting of these parameters could increase the SG width and hence promotes geometrical inaccuracy. Further, the stability of the SG width is adversely affected at high wire feed rate because of vibration and collision of wire with ceramic particles presence in the hybrid MMC workpiece.[25]

Estimation of predicted MRR and SG

Prior to performing confirmation experiments to verify the optimal conditions of input process parameters, confidence interval (CI) of predicted responses has been computed. The CIs for mean optimum values of MRR and SG were established using following mathematical models[39]

CI for MRR is as follows

$$\mathrm{CI_{MRR}} = \sqrt{F_\alpha(1,f_e)V_e\left[\frac{1}{n_{\mathrm{eff}}}+\frac{1}{R}\right]} \tag{5}$$

where

$$n_{\mathrm{eff}} = \frac{N}{1+T_{\mathrm{dof}}} \tag{6}$$

where, $F_e(1,f_e)$ is the F-ratio (95% confidence), α is the significance level, n_{eff} is showing effective no. of replications, R is the count of replications required for confirmatory experiments, N is the total experimental trials, and T_{dof} is taken to be the total DoF

$$T_{dof} = \text{number of factors} \times \text{DoF of each factor}$$

$F_{0.05}(1,14) = 4.60$, (from standard "F-test" table), $V_e = 0.2296$, $R = 3$, $T_{\mathrm{dof}} = 12$, and $n_{\mathrm{eff}} = 3.8577$, f_e (DoF for error) = 14 (refer Table 4), V_e = mean square variance for error = 0.2296 (refer Table 4). After inserting the unknown values in equations (5) and (6), the CI for MRR can be written as

$$n_{\mathrm{eff}} = \frac{N}{1+T_{\mathrm{dof}}} = 6.23$$

$$\mathrm{CI_{MRR}} = \sqrt{4.60 \times 0.2296 \times 0.4938} = \pm 0.722$$

Further, the predicted mean MRR at optimum conditions (such as $A_2B_3C_1D_3E_2F_3$) has been calculated using equation (7)

$$\mathrm{MRR_{exp.}} = A_2 + B_3 + C_1 + D_3 + E_2 + F_3 - 5T_{\mathrm{MRR}} \tag{7}$$

where T_{MRR} is 8.576 mm3/min (overall average of MRR corresponding to all the 81 set of experimentations). The calculated values of average MRR at optimum levels are $A_2 = 9.47$, $B_3 = 9.471$, $C_1 = 9.642$, $D_3 = 8.524$, $E_2 = 8.742$, and $F_3 = 8.745$ (refer Table 6). After substituting these values in equation (7), the mean optimum value of MRR is predicted as 11.714 mm^3/min.

Table 6. Means at three levels of control parameters for MRR and SG.

Level	I_p	T_{on}	T_{off}	W_F	W_T	SV
			MRR			
1	7.489	6.94	9.642	8.896	8.504	8.338
2	9.47	9.318	8.396	8.31	8.742	8.647
3	8.771	9.471	7.691	8.524	8.484	8.745
Delta	1.981	2.531	1.951	0.586	0.258	0.407
Rank	2	1	3	4	6	5
SG						
1	0.0202	0.0203	0.02338	0.02173	0.02204	0.02216
2	0.023	0.022	0.02226	0.02263	0.02259	0.02258
3	0.024	0.024	0.02167	0.02293	0.02267	0.02257
Delta	0.004	0.0039	0.00171	0.0012	0.00062	0.00042
Rank	1	2	3	4	5	6

MRR: material removal rate; SG: spark gap; I_p: pulse peak current; T_{on}: pulse-on-time; T_{off}: pulse-off-time; W_F: wire feed rate; W_T: wire tension; SV: set voltage.

The predicted optimal MRR at 95% confidence level should obey the condition given by equation (8)

$$[\mathrm{MRR_{opt}} - \mathrm{CI_{MRR}}] < \mathrm{MRR_{exp}} < [\mathrm{MRR_{opt}} + \mathrm{CI_{MRR}}] \tag{8}$$

$$10.992 < \mathrm{MRR_{exp.}} < 12.436$$

It has been found that the predicted value for MRR (11.714 mm^3/min) satisfies equation (8) at 95% confidence level. Similarly, the CI for predicted mean value of SG was computed following the same procedure. The input variables required in equations (5) and (6) are identified as: $F_{0.05}(1, 14) = 4.60$ (refer F-test), $V_e = 0.0000007$ (refer Table 5), $R = 3$, $T_{\mathrm{dof}} = 12$, and $n_{\mathrm{eff}} = 3$. The CI for SG can be written as

$$\mathrm{CI_{SG}} = \sqrt{4.60 \times 0.0000007 \times 0.4938} = 0.0012$$

Using Table 6, the mean SG at optimal condition is computed using equations (7) and (8)

$$\mathrm{SG_{opt}} = A_1 + B_1 + C_3 + D_1 + E_1 + F_1 - 5T_{SG}$$

$$[\mathrm{SG_{opt}} - \mathrm{CI_{SG}}] < \mathrm{SG_{exp}} < [\mathrm{SG_{opt}} + \mathrm{CI_{SG}}]$$

$$0.0147 < \mathrm{SG_{exp}} < 0.0171$$

Development of mathematical relations

To determine the correlations between a machining parameters and response characteristics, the multiple linear regressions were used and developed the mathematical relation for each of the responses. The regression function was evaluated to confirm the validity of the established mathematical models. Applying multiple linear regression analysis using MINITAB 17 software, the mathematical

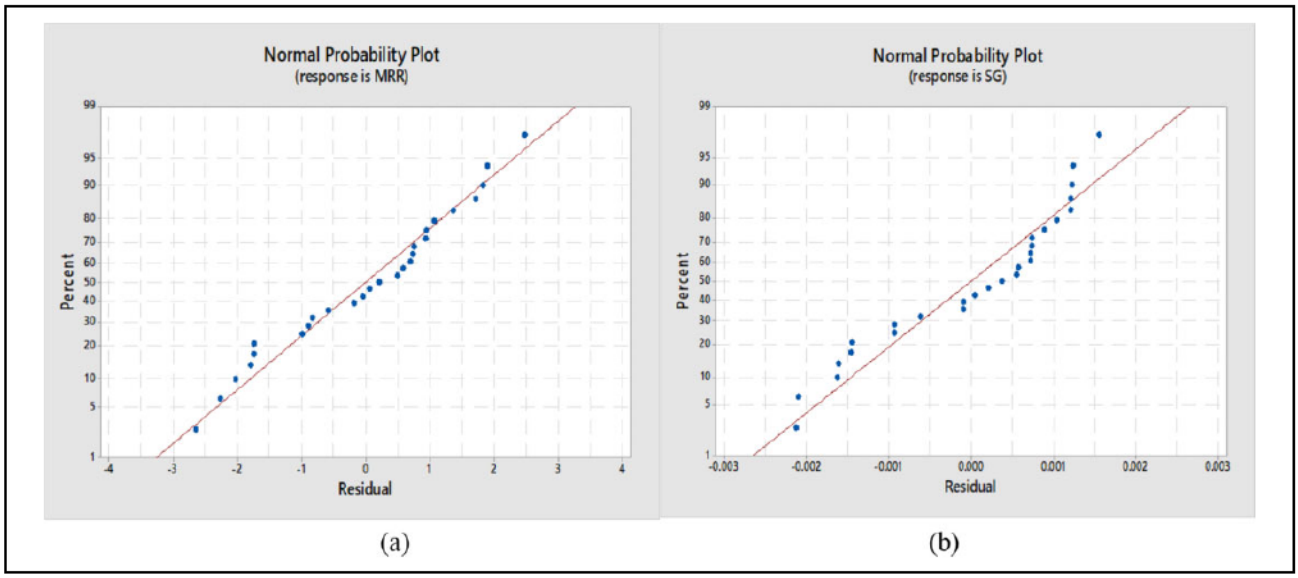

Figure 4. Normal probability plot for (a) MRR and (b) SG. MRR: material removal rate; SG: spark gap.

Table 7. Results of confirmatory experiments.

Response	Machining parametric combinations		Observed responses		Improvement (%)
	Initial machining parameters	Optimal parametric combination	Initial machining parameters	Optimal parametric combination	
MRR (mm^3/min)	$A_2B_2C_2D_2E_2F_2$	$A_2B_3C_1D_3E_2F_3$	8.54	11.4	33.72
SG (mm)	$A_2B_2C_2D_2E_2F_2$	$A_1B_1C_3D_3E_3F_1$	0.022	0.016	−27.28

MRR: material removal rate; SG: spark gap.

relations were developed to predict the responses, namely, MRR and SG. These developed mathematical relations can be directly utilized to predict the response values in advance within the given range of control parameters.

Mathematical relation for MRR and SG as evolved after machining are

$$Y_{MRR} = 5.45 + 0.0320I_p + 4.22T_{on} - 0.244T_{off} - 0.093W_F - 0.00012W_T + 0.0407\ SV$$

where $R^2 = 85.88\%$.

$$Y_{SG} = 0.00567 + 0.000099I_p + 0.00654T_{on} - 0.000214T_{off} + 0.000300W_F + 0.000002W_T + 0.000041\ SV$$

where $R^2 = 90.7\%$.

Furthermore, the normality assumptions are satisfied, if projection of residuals plot projects along a straight line.[38] The residuals for MRR and SG (refer Figure 4) lie apparently close to a straight line indicating that errors are distributed normally, and predicted values bear good agreement with experimental results.

The predicted response results are validated by performing confirmation experiments restricting to optimal levels of machining variables. The results obtained during confirmation experiment are presented in Table 7. The measurements of confirmation tests ($n = 3$) for MRR and SG have been conducted with regard to the respective optimal conditions. The corresponding values have been observed as 11.4 mm^3/min and 0.016 mm, respectively. Further, the mean observed values of MRR and SG falls within the determined CIs, for instance, $10.992 < MRR_{exp} < 12.436$ and $0.0147 < SG_{exp} < 0.0171$, respectively. Further, the predicted values are also very close to experimental results.

Examination of recast layer

Machined surface morphology plays a crucial role in improving the precision, reliability, and quality of the components. The cut surfaces produced by WEDM of the composites were sectioned in transverse direction for microstructure observations in machined areas. Figure 5(a) to (c) displays the workpiece machined microstructure image under the following machine settings: 120A—pulse peak current, 1.1 µs—pulse-on-time, 16 µs—pulse-off-time, 5 m/min—wire feed rate, 850 g—wire tension, and 35 V—SG voltage. At high setting of pulse peak current and pulse-on-time, it is generated enormous

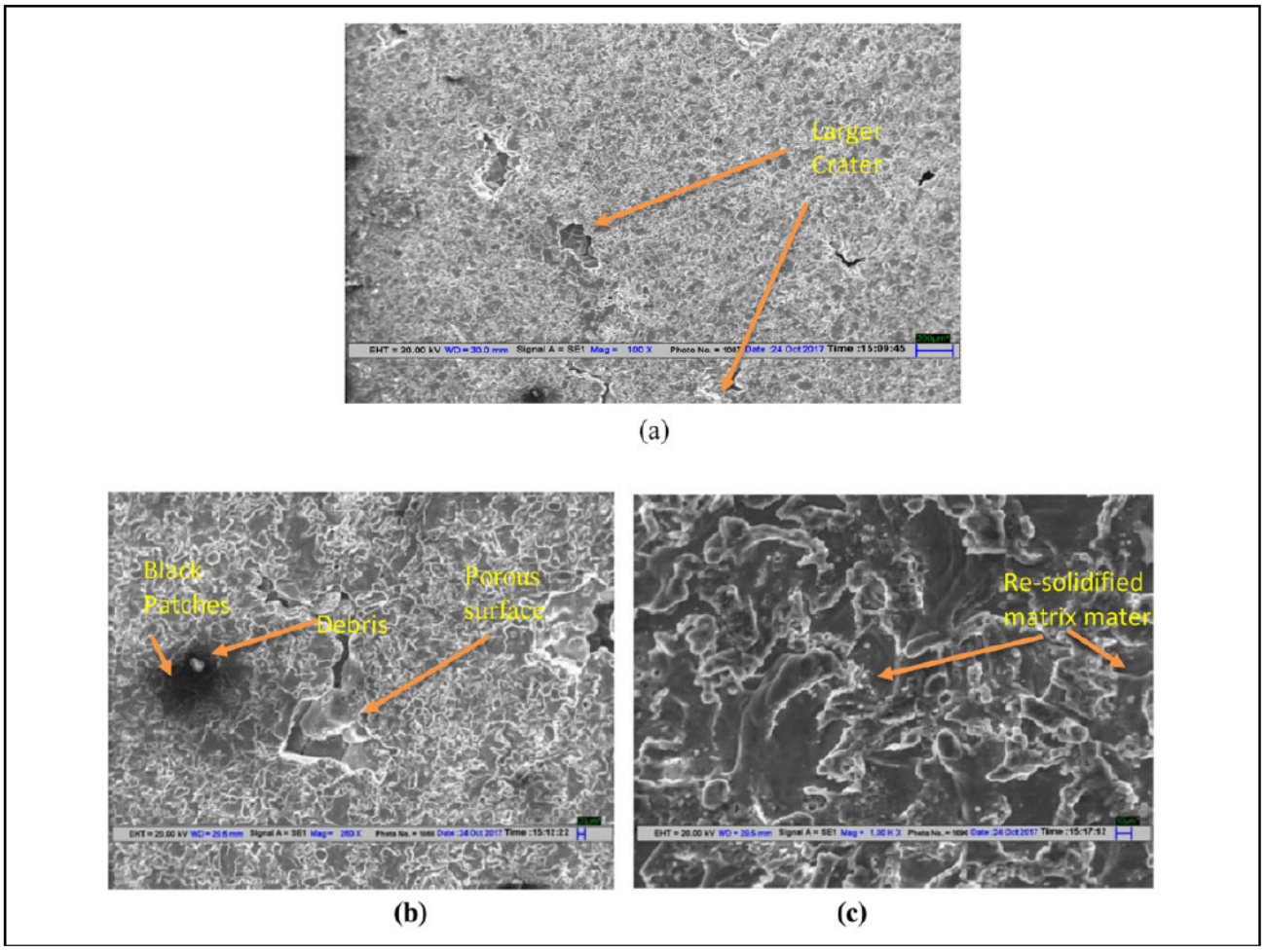

Figure 5. Machined surface at high pulse energy (1.1 μs—pulse-on-time and 120A—pulse peak current).

thermal energy during ionization phase. This raises up the local temperatures; eventually, the materials are melted and partially vaporized and flushed away by recirculating deionized water. Consequently, the tiny and large craters (Figure 5(a)) are also formed on the machining areas owing to the blasted out molten work by the discharge pressure. Grouping of individual tiny craters can be noticed, which probably are caused by raised up material temperatures. In turn do not permit sufficient time for dielectric cooling of an individual crater formed in due course before the next discharge occurs.[40] Subsequently, the surface moving away from spark zone attains the solidification temperature due to the presence of dielectric fluid and demonstrates the final surface structure (Figure 5). In addition to this, the material removal process also promotes the disintegration of the ceramic reinforcements to form large craters (Figure 5(a)). The increased pulse peak current and pulse-on-time exhibits a vital role in size of craters formed in the machining areas and other surface characteristics. Figure 5 depicts the formation of black patches besides the presence of formation of fine surface enveloped by tiny and shallow size craters. The black patches confirm the incidences of arcing occurred during machining owing to the presence of debris over the machined surface (Figure 5(b)).

EDS plotted in Figure 6(a) and (b) reveals the presence of oxygen. It is likely to increase with extended pulse-on-time. Oxygen is released owing to the disassociation of dielectric fluid (deionized water) at very high temperatures. Therefore, the porous surfaces have been spotted in the machined areas as can be noticed from Figure 6(a). Oxidation and decomposition process liberates a huge amount of gas due to more heat input by extended time intervals of discharges. This could cause more porous surfaces in the machined areas and therefore decreases the hardness and fracture toughness of the spark eroded surfaces. The EDS of the surface is also referred for elemental analysis which enables to determine the migration of electrode material to machined surface. EDS elemental maps in Figure 6(b) show that the machined work surface contains only elements of target material, namely, Al, carbon, oxygen, and magnesium, and Cu. The presence of element "Cu" indicates that partially melted wire electrode migrates on machined surface. The wire wear can increase the SR. The presence of Si in the machined surface was apparently

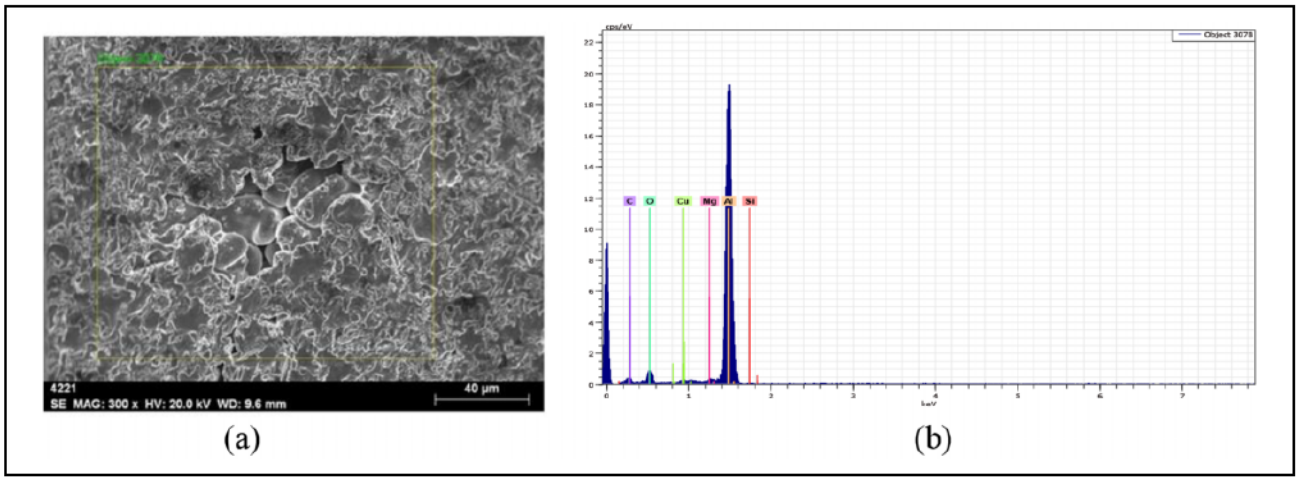

Figure 6. EDS analysis confirming migration of electrode material into recast layer. EDS: energy dispersive spectroscopy.

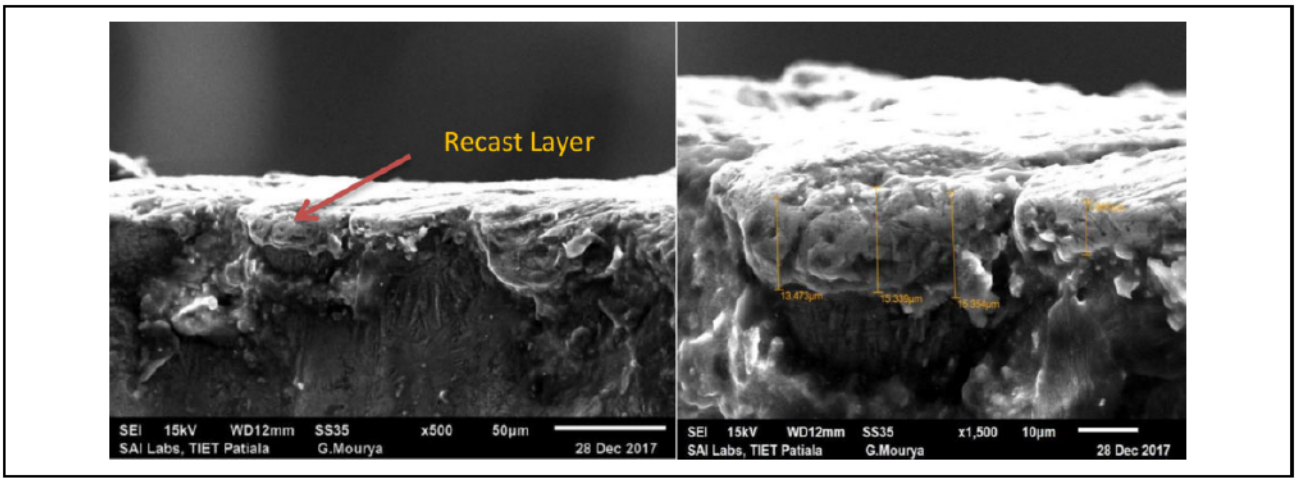

Figure 7. Recast layer formed on machined surface.

noticed which confirm disassociation of some SiC particles at high temperatures.[27]

The recast layer is formed by resolidification of the molten material which is not dispensed off by the flushing. This material is subjected to intense heating by the electrical discharges and rapid quenching by the dielectric fluid which can promote cracking and residual stresses. With higher energy release in each spark associated to an increased pulse energy, the amount of matrix material which is melted is higher results in a thicker recast layer as shown in Figure 7. The presence of ceramic particles in the work material and variation of spark energy has produced a nonuniformity in the recast layer. The recast layer is noticed to be fine grained and hard.

The residual stresses are another important consideration in understanding surface integrity of the machined surface. It is derived from material processing and machining history. The rapid metallurgical transformations and temperature gradient spikes in EDM process generate residual stresses in the recast layer.[41] These stresses sometimes exceed yield point of the target material and promote severe twining, slip, and cleavage subject to the type of crystal structure.[42] The residual stress significantly impacts the fatigue life of the machined components and also causes cracking or distortion in some cases, thereby leading to premature service failure. As mentioned earlier in this article, recast layer thickness grows to be thicker with increase in the pulse energy desired for high MRR, that is, rough cutting. Further, this growth in the average recast layer thickness induces more stress on the machined surface. Therefore, factors governing pulse energy, that is, pulse-on-time and peak current, are crucial for severity of induced residual stresses and crack formation. The absence of tearing cracks in softened machined surface by the local raised up temperature indicates that only compressive or moderate tensile residual stress is present in the recast layer.[43] Cracks are not clearly visible on the machined surface indicating that rapid dissipation of heat occurs from recast layer while machining takes place (Figure 5(a)). Yet, the finish machining is desired to achieve better surface

quality as material settled to higher stress during rough machining gets removed.[44] In future, the multi-objective optimization must be performed to reduce energy consumption and attain sustainable machining goals.[45,46]

Conclusions

The hybrid Al-MMCs samples were successfully fabricated using stir cast technique. The robust design of experiment technique has been applied to optimize the machining parameters affecting the considered responses. The effect of the important WEDM control parameters on MRR and SG width has been deeply analyzed and as well displayed graphically. Below are the main conclusions figured out through rigorous experimental study carried to investigate the WEDM machinability of newly developed MMC.

- Stir casting method appeared to be a flexible fabrication technique to prepare hybrid MMCs considering multiple reinforcements.
- WEDM machining method has been experienced to be a potential machining method to cut the Al hybrid MMCs irrespective of the high hardness and strength of the target material.
- For higher MRR, the optimum WEDM parametric combination has been identified as: 100 A—pulse peak current, 1.1 µs—pulse-on-time, 20 µs—pulse-off-time, 9 m/min—wire feed rate, 1000 g—wire tension, and 35 V—SG voltage. Further, for obtaining minimum SG, optimal parametric combination of WEDM is: 80A—pulse peak current, 0.5 µs—pulse-on-time, 20 µs—pulse-off-time, 5 m/min—wire feed rate, 850 g—wire tension, and 25 V—SG voltage.
- The improvement in MRR and SG at optimal parametric setting has resulted in an improvement of 33.72% and −27.28%, respectively.
- Pulse-on-time had most significant effect on MRR with contribution of 46.50%. However, pulse-peak current and pulse-off-time are also noticed to be statistically significant with contribution of 23.30% and 22.53% to MRR. It has been found that the most significant factors for SG are pulse peak current (53.02%) and pulse-on-time (50.79%). Likewise, pulse-off-time and wire feed rate also influence the SG, significantly.
- The developed mathematical relations for MRR and SG were used for a suitable selection of WEDM parameters leading to an effective machining of hybrid Al-MMCs.
- The SEM/EDS analysis revealed that the recast layer grows thicker with the increase of pulse-on-time, while the presence of reinforcements is the prominent reason for uneven thickness of recast layer. The EDS analysis of machined surface confirmed the migration of melted wire electrode material into recast layer.
- Cracks were not clearly visible on the machined surface indicating that rapid dissipation of heat occurs from recast layer while machining of hybrid Al MMC. The absence of tearing cracks in softened machined surface by the local raised up temperature indicates that only compressive or moderate tensile residual stress is present in the recast layer.

Declaration of conflicting interests

The author(s) declared no potential conflicts of interest with respect to the research, authorship, and/or publication of this article.

Funding

The author(s) received no financial support for the research, authorship, and/or publication of this article.

ORCID iD

Chander Prakash https://orcid.org/0000-0003-0856-9712
Catalin Iulian Pruncu https://orcid.org/0000-0002-4926-2189

References

1. Miracle DB. Metal matrix composites—from science to technological significance. *Compos Sci Technol* 2005; 65(15-16): 2526–2540.
2. Rajmohan T and Palanikumar K. Experimental investigation and analysis of thrust force in drilling hybrid metal matrix composites by coated carbide drills. *Mater Manuf Process* 2011; 26(8): 961–968.
3. Sharma DK, Mahant D, and Upadhyay G. Manufacturing of metal matrix composites: a state of review. *Mater Today: Proc* 2020; 26: 506–519.
4. Kumar S, Singh R, and Hashmi MS. Metal matrix composite: a methodological review. *Adv Mater Process Technol* 2020; 6(1): 13–24.
5. Suresha S and Sridhara BK. Friction characteristics of aluminium silicon carbide graphite hybrid composites. *Mater Des* 2012; 34: 576–583.
6. Ramanathan A, Krishnan PK, and Muraliraja R. A review on the production of metal matrix composites through stir casting—furnace design, properties, challenges, and research opportunities. *J Manuf Process* 2019; 42: 213–245.
7. Yigezu BS, Jha PK, and Mahapatra MM. The key attributes of synthesizing ceramic particulate reinforced Al-based matrix composites through stir casting process: a review. *Mater Manuf Process* 2013; 28(9): 969–979.
8. El-Gallab M and Sklad M. Machining of Al/SiC particulate metal matrix composites—part II: workpiece surface integrity. *J Mater Proc Technol* 1998; 83: 277–285.
9. Li J and Laghari RA. A review on machining and optimization of particle-reinforced metal matrix composites. *Int J Adv Manuf Technol* 2019; 100(9-12): 2929–2943.

10. Sahin Y and Sur G. The effect of Al_2O_3, TiN and Ti (C, N) based CVD coatings on tool wear in machining metal matrix composites. *Surf Coating Tech* 2004; 179(2–3): 349–355.
11. Kannan S, Kishawy HA, and Balazinski M. Flank wear progression during machining metal matrix composites. *J Manuf Sci Eng* 2006; 128: 787–791.
12. Niknam SA, Kamalizadeh S, Asgari A, et al. Turning titanium metal matrix composites (Ti-MMCs) with carbide and CBN inserts. *Int J Adv Manuf Technol* 2018; 97(1-4): 253–265.
13. Kannan S and Kishawy HA. Tribological aspects of machining aluminum metal matrix composites. *J Mater Process Technol* 2008; 198(1-3): 399–406.
14. Li G, Munir K, Wen C, et al. Machinablility of titanium matrix composites (TMC) reinforced with multi-walled carbon nanotubes. *J Manuf Process* 2020; 56: 131–146.
15. Manna A and Bhattacharayya B. A study on machinability of Al/SiC-MMC. *J Mater Process Technol* 2003; 140: 711–716.
16. Skibo MD and Schuster DM. High-speed, low-cost, machining of metal matrix composites. *Patent 6752709, USA, 2004*.
17. Manna A and Bhattacharyya B. Taguchi and Gauss elimination method: a dual response approach for parametric optimization of CNC wire cut EDM of PRAlSiCMMC. *Int J Adv Manuf Technol* 2006; 28(1-2): 67–75.
18. Garg RK, Singh KK, Sachdeva A, et al. Review of research work in sinking EDM and WEDM on metal matrix composite materials. *Int J Adv Manuf Technol* 2010; 50(5-8): 611–624.
19. Yue TM and Dai Y. Wire electrical discharge machining of Al_2O_3 particle and short fiber reinforced aluminum based composites. *Mater Sci Technol* 1996; 12: 831–835.
20. Gatto A and Iuliano L. Cutting mechanism and surface features of WED machined metal matrix composites. *J Mater Process Technol* 1997; 65: 209–214.
21. Rozenek M, Kozak J, Dabrowski L, et al. Electrical discharge machining characteristics of metal matrix composites. *J Mater Process Technol* 2001; 109(3): 367–370.
22. Yan BH, Tsai HC, Huang FY, et al. Examination of wire electrical discharge machining of Al_2O_{3p}/6061Al composites. *Int J Mach Tools Manuf* 2005; 45(3): 251–259.
23. Patil NG and Brahmankar PK. Some studies into wire electro-discharge machining of alumina particulate-reinforced aluminum matrix composites. *Int J Adv Manuf Technol* 2010; 48(5-8): 537–555.
24. Rahman M, Dey A, and Pandey KM. Machinability of cenosphere particulate–reinforced AA6061 aluminium alloy prepared by compocasting. *Proc Inst Mech Eng B: J Eng Manuf* 2018; 232(14): 2499–2509.
25. Kumar H, Manna A, and Kumar R. Modeling of process parameters for surface roughness and analysis of machined surface in WEDM of Al/SiC-MMC. *Trans Indian Inst Met* 2018; 71(1): 231–244.
26. Vijayabhaskar S and Rajmohan T. Experimental investigation and optimization of machining parameters in WEDM of nano-SiC particles reinforced magnesium matrix composites. *Silicon* 2019; 11(4): 1701–1716.
27. Pramanik A and Basak AK. Degradation of wire electrode during electrical discharge machining of metal matrix composites. *Wear* 2016; 346: 124–131.
28. Satishkumar D, Kanthababu M, Vajjiravelu V, et al. Investigation of wire electrical discharge machining characteristics of Al6063/SiC_p composites. *Int J Adv Manuf Technol* 2011; 56: 975–986. DOI: 10.1007/s00170-011-3242-5.
29. Pramanik A and Littlefair G. Wire EDM mechanism of MMCs with the variation of reinforced particle size. *Mater Manuf Process* 2016; 31(13): 1700–1708.
30. Gopal PM, Prakash KS, and Jayaraj S. WEDM of Mg/CRT/BN composites: effect of materials and machining parameters. *Mater Manuf Process* 2018; 33(1): 77–84.
31. Gopal PM. Wire electric discharge machining of silica rich E-waste CRT and BN reinforced hybrid magnesium MMC. *Silicon* 2019; 11(3): 1429–1440.
32. Kavimani V, Prakash KS, and Thankachan T. Multi-objective optimization in WEDM process of graphene—SiC-magnesium composite through hybrid techniques. *Measurement* 2019; 145: 335–349.
33. Meenakshi R and Suresh P. WEDM of Cu/WC/SiC composites: development and machining parameters using artificial immune system. *J Exp Nanosci* 2020; 15(1): 12–25.
34. Manna A, Bains HS, and Mahapatra PB. Experimental study on fabrication of Al—Al_2O_3/Gr_p metal matrix composites. *J Comp Mater* 2011; 45(19): 2003–2010.
35. Mandal A, Dixit AR, Das AK, et al. Modeling and optimization of machining nimonic C-263 superalloy using multicut strategy in WEDM. *Mater Manufact Process* 2016; 31(7): 860–868.
36. Çakiroglu R and Acir A. Optimization of cutting parameters on drill bit temperature in drilling by Taguchi method. *Measurement* 2013; 46(9): 3525–3531.
37. Sarıkaya M and Gullu A. Taguchi design and response surface methodology based analysis of machining parameters in CNC turning under MQL. *J Clean Prod* 2014; 65: 604–616.
38. Ong P, Chong CH, Bin Rahim MZ, et al. Intelligent approach for process modelling and optimization on electrical discharge machining of polycrystalline diamond. *J Intell Manuf* 2020; 31(1): 227–247.
39. Montgomery DC. *Design and analysis of experiments*. New York: Wiley, 2004
40. Newton TR, Melkote SN, Watkins TR, et al. Investigation of the effect of process parameters on the formation and characteristics of recast layer in wire-EDM of Inconel 718. *Mater Sci Eng: A* 2009; 513: 208–215.
41. Das S and Joshi SN. Estimation of wire strength based on residual stresses induced during wire electric discharge machining. *J Manuf Process* 2020; 53: 406–419.
42. Ekmekci B, Elkoca O, Erman Tekkaya A, et al. Residual stress state and hardness depth in electric discharge machining: de-ionized water as dielectric liquid. *Mach Sci Technol* 2005; 9(1): 39–61.

43. Salvati E and Korsunsky AM. Micro-scale measurement and FEM modelling of residual stresses in AA6082-T6 Al alloy generated by wire EDM cutting. *J Mater Processing Technol* 2020; 275: 116373.
44. Rahim MZ, Li G, Ding S, et al. Electrical discharge grinding versus abrasive grinding in polycrystalline diamond machining—tool quality and performance analysis. *Int J Adv Manuf Technol* 2016; 85(1-4): 263–277.
45. Bagaber SA and Yusoff AR. Multi-objective optimization of cutting parameters to minimize power consumption in dry turning of stainless steel 316. *J Clean Prod* 2017; 157: 30–46.
46. Pramanik A, Islam MN, Boswell B, et al. Accuracy and finish during wire electric discharge machining of metal matrix composites for different reinforcement size and machining conditions. *Proc Inst Mech Eng B: J Eng Manuf* 2018; 232(6): 1068–1078.